5th International Symposium on Three-Dimensional Electromagnetics
Sapporo, Japan, May 7-9, 2013

3D inversion of land-based CSEM data from the Ketzin CO_2 storage formation

Alexander Grayver[1], Rita Streich[1,2] and Oliver Ritter[1]
[1]GFZ German Research Center for Geosciences
[2]Now at Shell Global Solutions International

SUMMARY

We present 3D inversion of land CSEM data collected across the CO_2 storage test site at Ketzin, Germany. A newly developed Gauss-Newton type parallel distributed inversion scheme, which is based on a direct forward solver, is applied to recover subsurface conductivity images. Cumulative sensitivity volumes computed for the sparse CSEM survey geometry indicate reasonable spatial coverage along the main survey line. We fit the data to an uncertainty level obtained from robust data processing, and achieve a reasonable fit for most of the receivers. The principal features in the obtained 3D resistivity model are robust against the inversion parameterization and correlate well with the main geological units.

Keywords: land CSEM, 3D inversion, Gauss-Newton, case study

INTRODUCTION

Marine controlled-source electromagnetic (mCSEM) in the frequency domain has experienced extensive growth during the last decade, with hardware and analysis tools reaching mature stages of development (Constable 2010). In contrast, frequency-domain CSEM on land has rarely been attempted. Instead, time domain methods are commonly used, although recent comparisons (Connell and Key, 2012; Yang and Oldenburg, 2012) show similar resolution properties for both methods.

To a large extent, recently developed mCSEM methodology can be carried over to CSEM work on land, yet one also faces problems specific to land-based studies. For instance, we cannot expect the source-receiver coverage typical for mCSEM surveys, since arbitrary positioning of long transmitters and receivers on land is technically more difficult and typically restricted in populated areas. Therefore, sources are commonly operated over long times at fixed positions. This survey mode allows for recording wider frequency ranges, partly compensating for the sparser coverage. Furthermore, more sophisticated source configurations such as three-phase transmitters allow for acquiring data at various source polarizations (Streich et al., 2011). This would not be practical in marine settings.

The 3D inversion of land CSEM data poses further challenges. Without the presence of water attenuating airwave effects, ground responses are weaker compared to marine surveys. To resolve subsurface structure and prevent misinterpretations, highly accurate forward solutions need to be generated at the major conductivity contrast of the air-ground interface. Unlike relatively short towed marine sources, kilometre-long grounded wires of land sources cannot be approximated by idealized unit dipoles without introducing significant errors (Streich and Becken, 2011). To handle long sources accurately, we use a secondary-field approach in which the true source geometry is considered in the quasi-analytical computation of primary fields for layered models.

In the following sections, we first outline the field experiment and the newly developed 3D inversion scheme. We then describe a representative inversion setup that has been selected from inversion tests for various parameterizations because of its good data fit. We show the performance of the inversion and the resulting subsurface resistivity model for this setup.

FIELD EXPERIMENT

In a recent land CSEM survey carried out across the CO_2 injection test site in Ketzin, Germany (Streich et al., 2011), eight three-phase CSEM transmitters and 39 five-component receivers were deployed as shown in Figure 1a. The receiver line is approximately perpendicular to the main anticlinal structure present at the site. The collected data set contains five EM field components at frequencies in the range 1/32 – 150 Hz. For 3D inversion, we selected a data subset that is expected to contain most of the subsurface information, yet allows us to run many tests within reasonable times. Synthetic and real data indicate that the magnetic field components are not sensitive to resistive objects, whereas the electric field components can resolve both resistors and conductors. Therefore, we only use the horizontal electric field. We selected five frequencies in the range 1/16 – 6 Hz. Based on inspection of data uncertainty levels and data consistency along the receiver line and over frequencies, we drop data with estimated uncertainties higher than 12%. We also drop data for receivers within 700 m of the source electrode positions, because near-source data can be strongly influenced by

local near-surface inhomogeneity and has little sensitivity to deeper structure. The data subset used in the inversion contains 3957 complex data values.

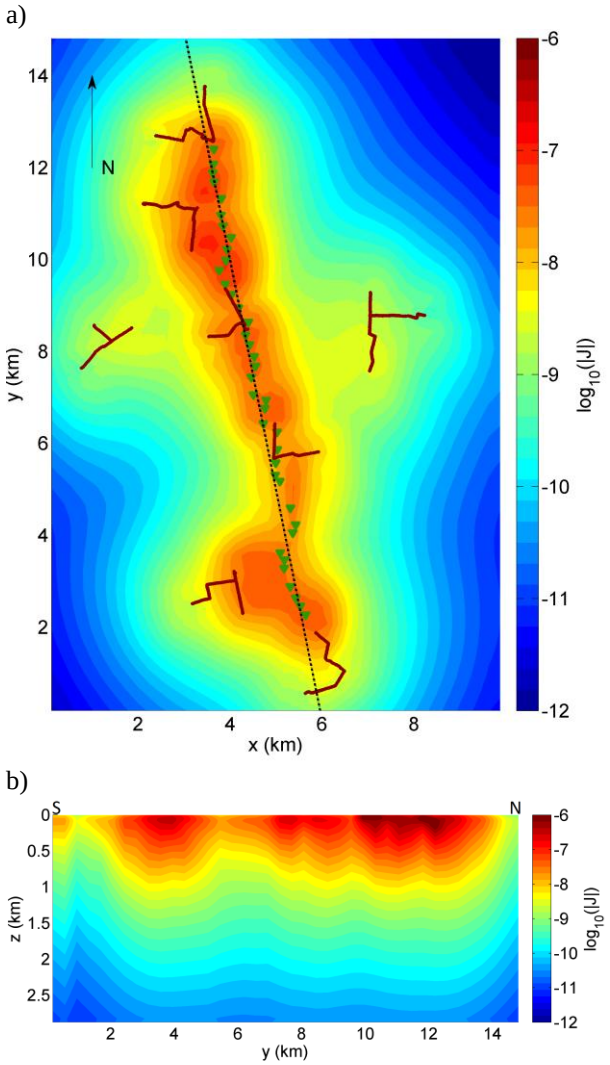

Figure 1. Field layout of the Ketzin survey, with green triangles indicating receivers and red lines indicating transmitters, and logarithm of cumulative sensitivity computed for a 5-Ωm homogeneous half-space and the inversion dataset. (a) Horizontal section at z = 0.6 km; (b) vertical section along the line depicted in (a).

Cumulative sensitivities computed for this data set indicate maximum resolution along the profile (Figure 1). At the CO_2 injection depth of ~630 m, sensitivities reach ~10% of the maximum near-surface values.

INVERSION

Algorithm

A newly developed fully distributed 3D inversion scheme is applied to invert the data (Grayver et al., 2012). The inversion uses a Gauss-Newton minimization scheme (Newman and Hoversten, 2000) with bounded conductivity transforms (Kim and Kim, 2011) and computation of the full Jacobian. The code makes extensive use of the PETSc library (Balay et al., 2011) and its interface to MUMPS (Amestoy et al., 2006) for distributed linear algebra. This ensures that memory and workload are distributed approximately evenly over all processes. Furthermore, the model is divided into subdomains for parallel calculation of primary fields for realistic sources.

Field data inversion

We started the inversion from a 5-Ωm homogeneous half-space. All model parameters were constrained such that $0.25 < \rho < 10^4$ Ωm. The inversion grid consisted of 40 x 40 x 60 cells with horizontally uniform sizes of 250 x 375 m and variable cell sizes in z dimension. A smoothing regularization was used to stabilize the inversion. To prevent inversion artefacts caused by numerical singularities at the sources, the conductivity at the source locations has to be included in the background conductivity model, and all cells transected by the wires of one source should have identical conductivities. Therefore, we placed the sources into a 5-m thick layer at the air-ground interface that was kept constant at each iteration. The inversion was stopped after 25 iterations, reaching an overall relative misfit of 13.5 (Figure 2).

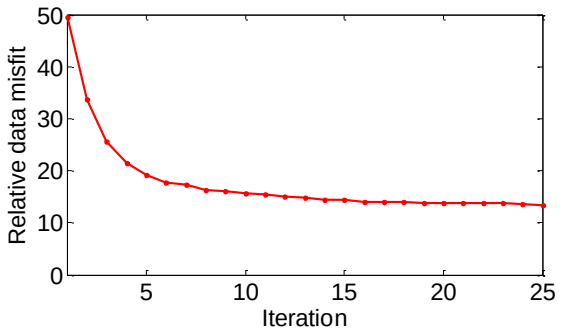

Figure 2. Relative data misfit versus iteration count during the inversion.

Inspection of the individual misfits for each receiver reveals that we generally reduce the misfits 6-7 times for all receivers except for those located in the center of the profile between ~6–8 km. These data are particularly severely affected by noise from a nearby transformer station and a gas pipeline carrying pulsed anticorrosion currents that crosses the receiver line at ~7 km.

Figure 4 shows resistivities obtained from the 3D inversion along the receiver line. The image contains several prominent conductive and resistive horizontally continuous structures that also appeared nearly identically for different inversion setups. The regional geological is well constrained, with an anticline structure of sediments overlying a salt pillow (Förster et al., 2009). The top of the anticline is at a depth of approximately

2 km near the center of our survey line. The electrical conductivity structures recovered by 3D CSEM inversion correlate well with the main geological units (see Fig. 4).

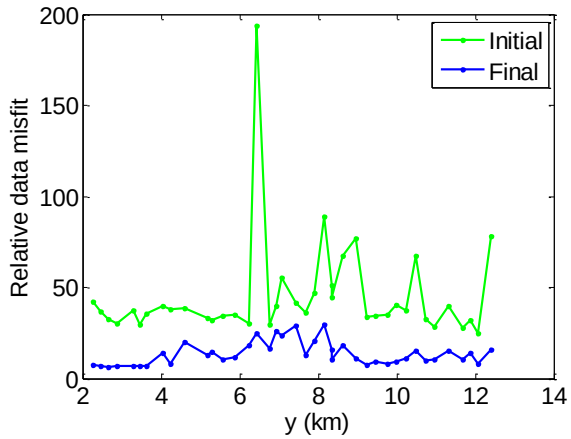

Figure 3. Initial and final data misfits for each receiver with respect to all frequencies and transmitters.

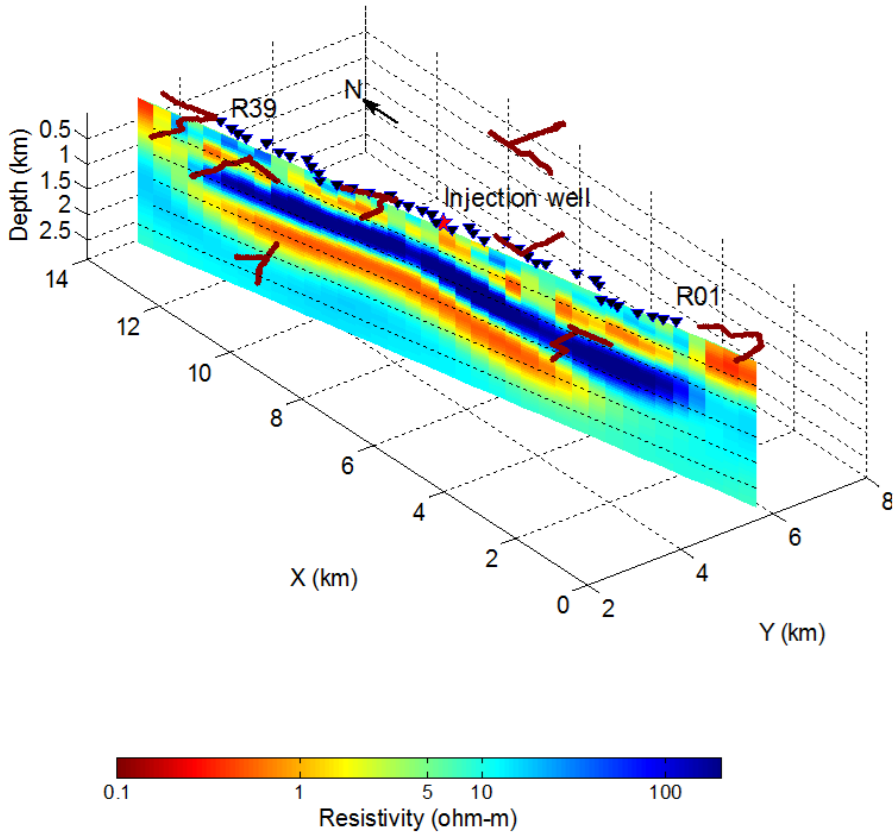

Figure 4. Section extracted from the 3D inversion model along the receiver line. Red lines and black triangles indicate transmitters and receivers, respectively. The red star shows the position of the CO_2 injection well.

The inversion was run using 64 processes on four interconnected cluster nodes, each equipped with two twelve-core AMD Opteron processors and 64 GB RAM. One iteration took approximately 2.5 hours, and the total memory usage did not exceed 50 GB.

CONCLUSIONS

We have successfully applied 3D inversion to real land-based CSEM data. Without considering any geological *a priori* information by starting from a homogeneous halfspace, the Gauss-Newton minimization scheme achieves a good data fit and arrives at a resistivity model that agrees well with the known geological structures.

Using distributed computations extensively, we are able to run the computationally expensive direct-solver-based 3D Gauss-Newton inversion in reasonable times. The field data inversion results also demonstrate that the inversion scheme can handle practically relevant problems on moderate-size computational platforms that are widely available now.

ACKNOWLEDGMENTS

This work is part of the MULTI-EM project, which is funded by the German Ministry of Education and Research, Grant 03G0746A-MULTI-EM. The Ketzin

dataset was collected within the GeoEn project with the invaluable help of the GFZ Potsdam EM research group and students.

REFERENCES

Amestoy, P. R., Guermouche, A., LExcellent, J.-Y., and Pralet, S., 2006, Hybrid scheduling for the parallel solution of linear systems, *Parallel Computing*, **32**, 136–156.

Balay, S., Brown, J., Buschelman, K., Eijkhout, V., Gropp, W. D., Kaushik, D., Knepley, M. G., McInnes, L. C., Smith, B. F., and Zhang, H., 2011, PETSc user's manual, *Technical Report ANL-95/11 - Revision 3.2*, Argonne National Laboratory.

Connell, D., and Key, K., 2013, A numerical comparison of time and frequency-domain marine EM methods for hydrocarbon exploration in shallow water, *Geophysical Prospecting*, in press.

Constable, S., 2010, Ten years of marine CSEM for hydrocarbon exploration, *Geophysics*, **75**, A67-A81.

Förster, A., Giese, R., Juhlin, C., Norden, B. Springer, N., 2009, The Geology of the CO2SINK Site: From Regional Scale to Laboratory Scale, *Energy Procedia*, **1**, 2911-2918.

Grayver, A. V., Streich, R., and Ritter, O., 2012, Three-dimensional parallel distributed inversion of CSEM data using a direct forward solver, *Geophysical Journal International*, submitted.

Kim, J. H., and Kim, Y., 2011. A unified transformation function for lower and upper bounding constraints on model parameters in electrical and electromagnetic inversion, *Journal of Geophysics and Engineering*, **8**, 21–26.

Newman, G., and Hoversten, M., 2000. Solution strategies for two- and three-dimensional electromagnetic inverse problems, *Inverse Problems*, **16**, 1357–1375.

Streich, R., and Becken, M., 2011, Electromagnetic fields generated by finite-length wire sources: comparison with point dipole solutions, *Geophysical Prospecting*, **59**, 361–374.

Streich, R., Becken, M., Matzander, U., and Ritter, O., 2011, Strategies for land-based controlled-source electromagnetic surveying in high-noise regions, *The Leading Edge*, **30**, 1174–1181.

Yang, D., and Oldenburg, D. W., 2012, Three-dimensional inversion of airborne time-domain electromagnetic data with applications to a porphyry deposit, *Geophysics*, **77**, B23–B34.